8-band k.p modeling of the quantum confined Stark effect in Ge quantum wells on Si substrates

D. J. Paul*

Department of Electronics and Electrical Engineering, University of Glasgow, Oakfield Avenue, Glasgow G12 8LT, United Kingdom

(Received 29 November 2007; published 24 April 2008)

Recent work using compressively strained-Ge quantum wells grown on $Si_{1-y}Ge_y$ virtual substrates has demonstrated efficient modulation on a silicon substrate through the quantum confined Stark effect with performance comparable to many direct band gap III-V materials. The absorption of compressively strained-Ge quantum wells is calculated by using an 8-band **k.p** solver within the envelope function technique. The calculated absorption spectra provide excellent agreement with experimental results, demonstrating that the absorption is dominated by the direct band gap, and allow a number of predictions of the absorption for different polarizations, quantum well widths, electric fields, and strain to be calculated. It is also shown that some of the experimental results in the literature require tensile strained substrates to produce agreement with the theoretical calculations.

DOI: 10.1103/PhysRevB.77.155323 PACS number(s): 71.35.Cc, 73.21.Fg, 78.20.Bh

I. INTRODUCTION

While silicon dominates the electronics market, the lack of an efficient light emitter or modulation effect has prevented complete silicon optoelectronic solutions from being realized. The indirect band gap of silicon results in significantly smaller electro-optical effects[1,2] than those in direct band gap III-V materials. Silicon photonics as a field has grown enormously in the last decade especially as copper interconnects on and off silicon chips are close to reaching the theoretical maximum bandwidths and new optical solutions are required for low cost, higher bandwidth performance from microelectronic systems.[2] Modulators have been demonstrated on silicon using the Franz-Keldysh effect[2] and the stronger free carrier plasma effect,[1–4] but all demonstrated devices still have poorer performance or larger sizes than equivalent III-V devices at the important 1.55 μm operating wavelength.

Recently, the quantum confined Stark effect (QCSE) was demonstrated by using strained-Ge quantum wells grown on top of a silicon wafer.[5,6] The QCSE can be considered as the analog of the Franz-Keldysh effect for electrons and holes confined in a type I quantum well so that bound excitonic effects strongly affect the absorption properties of the device.[7,8] The work on strained-Ge quantum wells[9] suggests that the direct electron Γ-valley transitions to hole states dominate the optical absorption properties of these systems as the zone-center Γ_{7c}^{-} valley for electrons is only about 140 meV above the L-valley conduction band edge.

In this paper, the absorption of compressively strained-Ge quantum wells is calculated by using an 8-band **k.p** solver.[10] The results demonstrate that the absorption is indeed dominated by the direct band gap and the modeling tool is used to calculate the absorption edge for a number of different quantum well widths and strain conditions. The polarization dependence of the absorption is also calculated demonstrating the difference between surface-normal (xy-polarization) and ridge waveguide (z-polarization) devices. One major issue that will be demonstrated is that a number of the published results require a strained virtual substrate rather than an unstrained virtual substrate to agree with the theory.

II. DESCRIPTION OF MODELING TECHNIQUE

The absorption was calculated by using the band structure tool NEXTNANO[10] using an 8-band **k.p** solver. The technique is similar to the envelope function technique derived by Bastard[11] and a full derivation of the absorption coefficient: $\alpha(\omega)$ as a function of angular frequency, ω can be found in Ref. 10. The basis states are S-like for the Γ_{7c}^{-}-conduction band and P-like for the valence band with each state with spin degeneracy of 2 giving the eight bands of $|S\uparrow\rangle$, $|X\uparrow\rangle$, $|Y\uparrow\rangle$, $|Z\uparrow\rangle$, $|S\downarrow\rangle$, $|X\downarrow\rangle$, $|Y\downarrow\rangle$, and $|Z\downarrow\rangle$. The absorption result is from the projection of the susceptibility tensor χ_{ij} onto the polarization vector ε_j of the incident light to produce

$$\alpha(\omega) = \frac{4\pi\omega}{nc}\varepsilon_i^* \chi_{ij}(\omega)\varepsilon_j, \tag{1}$$

where n is the refractive index and c is the speed of light. The susceptibility (only the imaginary part is required for absorption and is quoted after symmetry and selection rules have been used to reduce the form) is given by

$$\chi_{ij}(\omega) = \frac{i\pi e^2\hbar^2}{m^2\omega^2\Omega}\frac{1}{4\pi\varepsilon_0}\frac{E_p m_0}{2\hbar^2}\frac{S}{a_0^2}\left(\frac{a_0 k_{max}}{\pi}\right)^2 \times \sum_{n,n',\sigma}\int d\mathbf{k}_\perp |\langle n,k,\sigma,i|n',k,\sigma,i\rangle^* \times \langle n,k,\sigma,j|n',k,\sigma,j\rangle|^2 \tag{2}$$

for a transition from state n to n' at wave number k with spin σ and polarization i or j. The variables above are as follows: e is the electronic charge, $\hbar$ is Planck's constant divided by 2π, m is the effective mass, m_0 is the free electron mass, E_p is the Kane matrix element defined in terms of the momentum Hamiltonian as $\frac{2}{m_0}|\langle S\downarrow|\hat{p}_x|X\downarrow\rangle|^2$, S is the Kane parameter, a_0 is the Bohr radius, k_{max} is the maximum $k_\parallel$ wave number, ε_0 is the permittivity of free space, and Ω is the volume of the sample.

The major input parameters for the calculations are listed in Table I. Where possible, experimentally derived or measured input parameters have been used[12] although these were not available for a number of parameters. Unlike direct band

TABLE I. The input parameters used in the 8-band **k**.**p** modeling.

Parameter	Silicon	Germanium
Lattice constant, a (nm)	0.54304[a]	0.56579[a]
Elastic constant, c_{11} (GPa)	165.77[a]	128.53[a]
Elastic constant, c_{12} (GPa)	63.93[a]	48.28[a]
Elastic constant, c_{44} (GPa)	79.62[a]	66.80[a]
Varshni α_Γ (meV/K)	0.5367[b]	0.6842[b]
Varshni β_Γ (K)	745.8[b]	398[b]
Varshni α_L (meV/K)	0.5367[b]	0.4561[b]
Varshni β_L (K)	745.8[b]	210[b]
Kane matrix element, E_p (eV)	26.92[a]	25.49[a]
Kane parameter, S (eV)	1	1
a_v (eV)	1.80[c]	1.24[c]
b (eV)	−2.10[d]	−2.86[e]
d (eV)	−4.85[d]	−5.28[e]
a_c^Γ (eV)	−10.39[f]	−10.41[f]
a_c^L (eV)	−0.66[g]	−1.54[g]
a_c^X (eV)	3.3[h]	2.55[g]
Ξ_u^Γ	0.0	0.0
Ξ_u^L	16.14[g]	16.2[i]
Ξ_u^Δ	8.6[d]	9.42[g]
L' $(\hbar^2/2m^*)$	−6.69[j]	−31.34[j]
M' $(\hbar^2/2m^*)$	−4.62[j]	−5.90[j]
N' $(\hbar^2/2m^*)$	−8.56[j]	−34.14[j]
Δ (meV)	44[a]	289[a]

[a]Reference 14.
[b]Reference 15.
[c]Reference 16.
[d]Reference 17.
[e]Reference 18.
[f]Reference 19.
[g]Reference 20.
[h]Reference 21.
[i]Reference 22.
[j]Reference 23.

gap III-V materials that have a large literature of parameters for 8-band **k**.**p** tools,[13] the indirect materials of Si and Ge make the extraction of some of these parameters difficult.[12] For this work, the standard 6-band Dresselhaus parameters from Ref. 23 were used and they were not scaled to the 8-band values as described in Ref. 10 for III-V materials. The inversion symmetry operator was set to zero, the Kane parameter S was set to 1 eV, and the values of the Kane matrix element E_p were derived at 4.2 K for Si and 10 K for Ge by using experimental data from Ref. 12. All values were linearly extrapolated between Si and Ge values for $Si_{1-x}Ge_x$ layers except the Dresselhaus parameters which were bowed using the scheme in Ref. 23 since these values provide excellent agreement between the simulations and experimental intersubband hole absorption and emission results in Refs. 24–27. The coupling between the conduction and valence bands is therefore dominated by the Kane matrix element E_p in the present work. While some of these parameters are not used in the standard III-V way for 8-band **k**.**p** simulations,[13] the agreement between experiment and theory, which will be demonstrated later, provides the justification for the selection and present use of the parameters.

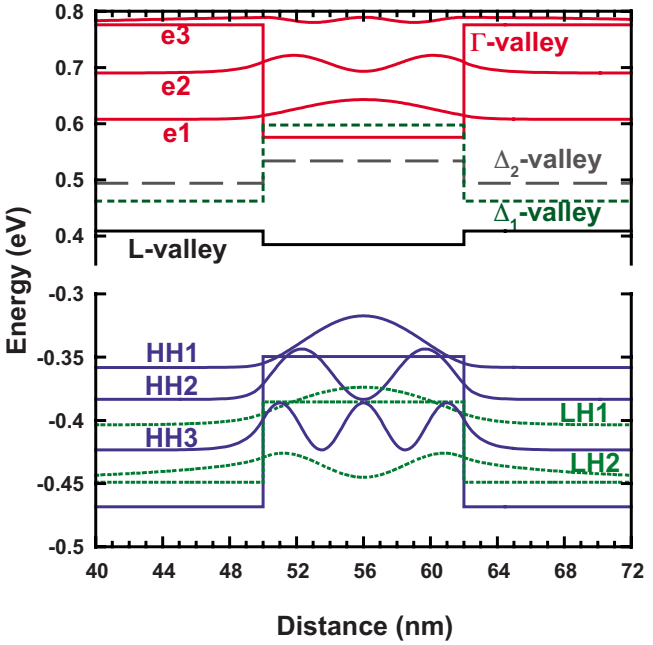

FIG. 1. (Color online) The band structure for the compressively strained 12 nm quantum well (Ref. 9) showing the band edges and squared wave functions for the lowest energy subband states for the Γ_{7c}^-, HH, and LH subbands.

III. DEVICES WITHOUT ELECTRIC FIELDS

The first structure to be modeled was a 12 nm compressively strained-Ge quantum well sandwiched between 24 nm thick tensile strained-$Si_{0.15}Ge_{0.85}$ barriers and grown on top of a linearly graded, relaxed $Si_{0.1}Ge_{0.9}$ virtual substrate.[9] For this particular structure, the experimental results in Ref. 9 are for flat band conditions without an applied electric field at 17 K. Figure 1 shows the calculated band edges and lowest energy subband states for the heavy-hole (HH), light-hole (LH), and Γ_{7c}^- conduction band electrons. Also shown are the band edges for the L and Δ valleys. The split-off (SO) band is too low in energy to be plotted and does not play any significant role in the absorption process although as with all strained-SiGe structures, there is significant mixing between the SO and LH states due to the off diagonal terms in the 8-band Hamiltonian. While strictly speaking these should be described as LH/SO subbands, for brevity they will be described as LH states from now on.

Figure 2 shows the in-plane dispersion of both the electron and hole subband states for those closest to the band edge transitions. While the electron dispersions are close to parabolic, the hole states are clearly nonparabolic. The selection rules assuming parabolic dispersions of the subbands with the xy polarization (TE) of the present experimental results allow the following transitions:[11] HH1-e1, HH2-e2, LH1-e1, LH2-e2, etc. While nonparabolicity can allow weak

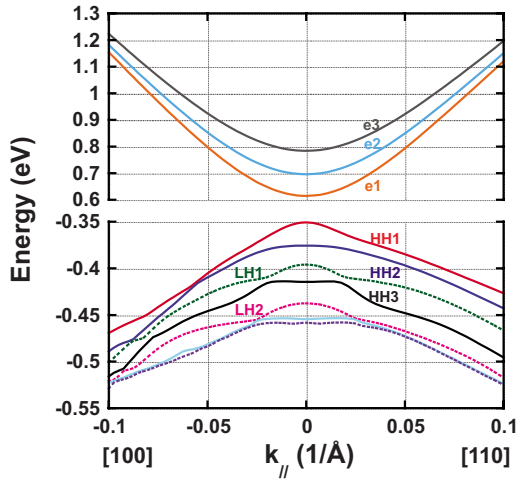

FIG. 2. (Color online) The in-plane subband dispersion of the electron and hole states along the [100] and [110] directions.

transitions at finite $k_{\|}$ from forbidden transitions in the parabolic approximation, in this work, none of the calculated absorption spectra show any significant absorption from relaxation of those forbidden transitions for the main excitonic features.

The absorption spectra were calculated up to a maximum k-parallel value of 1.1 nm^{-1} with 961 k-parallel points for the Brillouin zone discretization. Spectra were calculated for one, two, and five quantum wells with little difference being found in the calculated absorption spectra for different numbers of quantum wells. Hence, all subsequent absorption spectra will be calculated using a single quantum well which has the minimum computational resource requirements. Figure 3 shows the absorption spectra at 17 K for a single quantum well and spacers of 20 nm on each side of the quantum well assuming 1 meV of broadening compared to the experimental results in Ref. 9. The main transitions are also annotated on the figure and excellent agreement is shown between the calculated and experimental spectra for many of these transitions.

The experimental data in Fig. 3 were compared to absorption spectra calculated by 6-band **k**.**p** for the hole states and a single-electron effective mass calculation for the electrons in the original paper.[9] While this calculation produced excellent agreement for the lowest absorption peak experimentally observed at 0.978 eV, many of the other transitions were at significantly different energies to the experimental results. The present 8-band solutions using literature input values and no fitting parameters produce the first absorption peak at 0.973 eV and have better agreement with the higher transitions as would be expected with the addition of coupling between the electron and hole states. The present calculations also reproduce the absorption peak around 1.25 eV by extending the eigenvalue calculation to a 20 nm layer adjacent to the spacer and quantum well system with the composition of the relaxed $Si_{0.1}Ge_{0.9}$ virtual substrate. This peak was missing in the 6-band calculation[9] which only calculated the absorption for the Ge quantum well.

At present, the model uses a linear interpolation between Si and Ge for the band gap energy that produces the

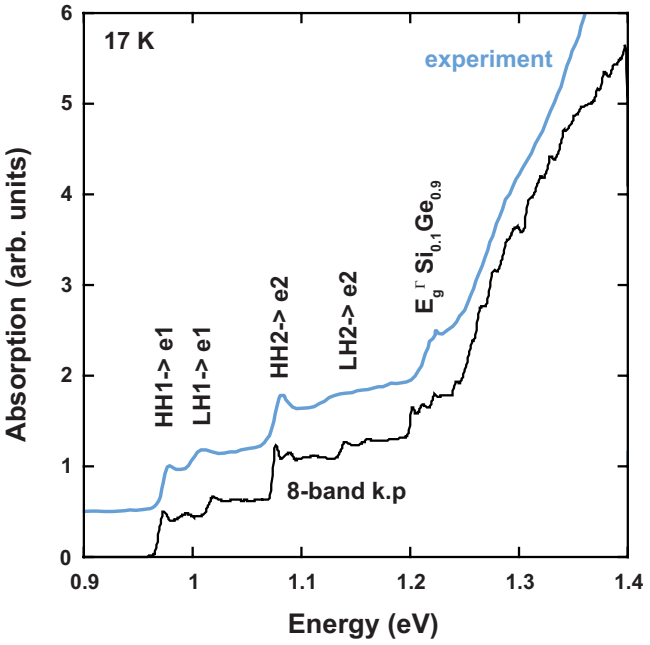

FIG. 3. (Color online) The xy-polarized spectra for the 12 nm Ge quantum well grown on $Si_{0.1}Ge_{0.9}$ virtual substrate with $Si_{0.15}Ge_{0.85}$ barriers and 0 V/m electric field at 17 K from Ref. 9. The curves are offset for clarity.

$Si_{0.1}Ge_{0.9}$ virtual substrate absorption peak close to 1.20 eV compared to the experimental 1.25 eV suggesting that bowing of the band gap energy is required for more accurate modeling of the substrate peak. The electron to HH absorption peaks is more accurately calculated by the model than the transitions to LH states. The HH subband state energies are related to first order to the well widths, while the energies of the LH states are much more related to the Ge content and are more strain dependent. The poorer fit to the electron to LH transitions also suggests that accurate bowing parameters are required for the band gap, which are the deformation and the Dresselhaus parameters, to provide more accurate predictions. At present, there is little $Si_{1-x}Ge_x$ data in the literature at these high Ge contents to allow accurate parameters to be experimentally determined.

The modeled absorption curve in Fig. 3 also shows very weak transitions at some of the forbidden transitions that are not observed in the experimental results. First, the modeled curve could have a larger smoothing factor added that would more closely resemble the experimental results, but the nonparabolicity that is required to break the selection rules may be different in the real sample compared to the model due to the bowing of the parameters discussed in the previous paragraph. Also above about 1.25 eV, the modeled curve shows discrete transitions due to the finite number of states calculated, which could be smoothed out by greatly increasing the number of quantum state solutions for the continuum but at the expense of greatly increased computational time.

The temperature dependence of the absorption spectra was also calculated by using the model of Varshni[27] to account for the change in band gap where

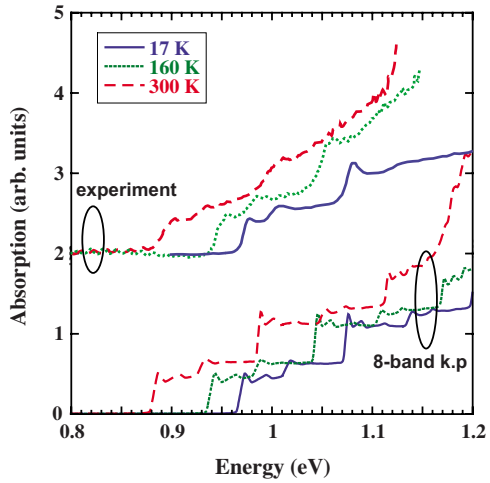

FIG. 4. (Color online) The temperature dependence of the *xy*-polarized spectrum as a function of temperature for the 12 nm Ge quantum well grown on $Si_{0.1}Ge_{0.9}$ virtual substrate with $Si_{0.15}Ge_{0.85}$ barriers and 0 V/m electric field from Ref. 9.

$$E_g(T) = E_g(T=0) - \frac{\alpha T^2}{T+\beta}. \tag{3}$$

The data used for the band gaps at different symmetry points and the fitting parameters, α and β, are listed in Table I and the resulting absorption spectra calculated using the data are compared to experiment in Fig. 4. The agreement for the absorption edge from 17 to 300 K is excellent even though no additional broadening over the 1 meV value has been added to the higher temperature calculations. It is clear that some form of additional broadening is required, especially for the higher energy transitions, if better fitting is required to the experimental data. The present results suggest that the broadening increases with temperature, but there are also, as will be discussed later, indirect absorption effects that also increase with increasing temperature.

IV. DEVICES WITH ELECTRIC FIELDS

The original paper on the Ge well QCSE used ten quantum wells inside a *p-i-n* structure that results in a built in electric field of 1.63 MV/m with 0 V applied across the *p-i-n* device.[5] The distance between *p*- and *n*-contact regions was 460 nm. To model this structure, a single quantum well was used with a constant electric field applied across the structure before the eigenstates were calculated. The calculated absorption spectrum is compared to the experimental data in Fig. 5. It was clear from the initial calculation of compressive-Ge quantum well and tensile spacers that being commensurate to a relaxed $Si_{0.1}Ge_{0.9}$ substrate (0% strain in Fig. 5) did not match the experimental data. Unlike the first sample from Ref. 9, which was grown on an ~13 μm thick linearly graded strain relaxation buffer where the grading rate was 7% Ge/μm, the experimental data in Fig. 5 came from a sample with a thin virtual substrate of only 500 nm thickness.[12] This thin buffer was grown at low temperature and then annealed at high temperature to relax. A number of papers[28,29] have demonstrated that such fabrication results in

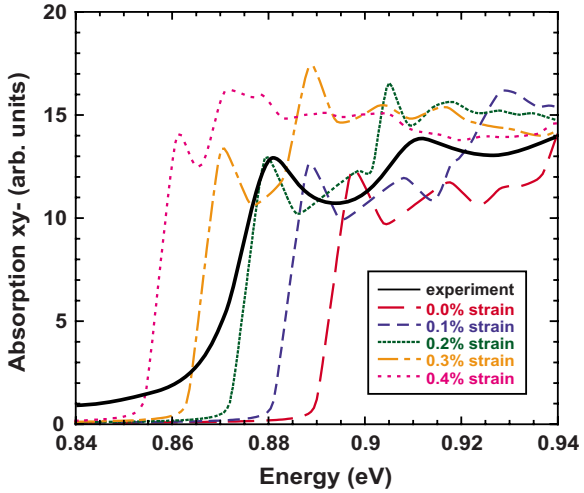

FIG. 5. (Color online) The *xy*-polarized absorption spectrum at 300 K for a 10 nm Ge quantum well on a $Si_{0.1}Ge_{0.9}$ virtual substrate with $Si_{0.15}Ge_{0.85}$ barriers with an electric field of 1.63 MV/m at 300 K. The solid black line is experimental data plotted from Ref. 5, while the dashed colored lines are for the 8-band $\mathbf{k}\cdot\mathbf{p}$ solutions with different levels of tensile strained substrate.

tensile strain and not complete relaxation in the buffer, and therefore the lattice constant is not that of bulk, relaxed $Si_{0.1}Ge_{0.9}$. Up to 0.2% tensile strain has been demonstrated just by annealing Ge heterolayers, while the addition of further processing steps such as backside silicidation has shown tensile strain up to 0.25%.[28]

To account for this tensile strain, the absorption spectra were calculated for different levels of tensile strain in the virtual substrate. This was achieved by calculating the appropriate lattice constant for each level of tensile strain in a $Si_{0.1}Ge_{0.9}$ layer and then fixing the substrate lattice constant to this value before commensurately straining the quantum wells, barriers, and spacers on top. The results for tensile strain levels in the substrate from 0% to 0.4% are plotted against the experimental results in Fig. 5 and the best fit for the main HH1-e1 absorption peak was obtained using 0.2% tensile strain. This is very similar to the values reported for similar strain relaxation buffers made out of pure Ge in Ref. 28 rather than $Si_{0.1}Ge_{0.9}$. For operation of modulators at the important 1.55 μm band (0.807 eV), tensile strain is beneficial in moving the absorption edge to lower energy or longer wavelength. It is also clear from Fig. 5 that the experimental results have a significantly larger tail below the HH1-e1 absorption peak than the modeled results. Expanding the broadening of the peak did not allow accurate modeling of this tail and it is believed to be related to indirect absorption between the *L* valley and hole states.

Figure 6 compares the experimental and modeled results for absorption as a function of applied bias for the 10 nm Ge-quantum-well modulator in Ref. 5. The calculated absorption shows good agreement with the experiment although that agreement becomes poorer as the voltage, and therefore electric field, is increased. This is not surprising as the larger electric fields will result in more heating in the sample and this would result in a higher probability of indirect absorption with the larger number of phonons in the

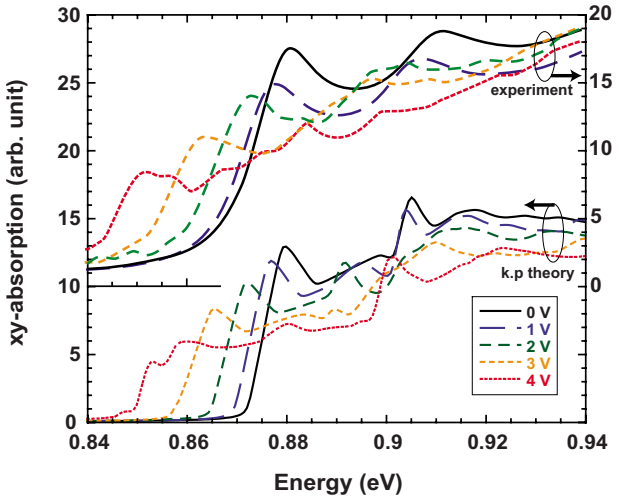

FIG. 6. (Color online) The *xy*-polarized absorption spectrum at 300 K for a 10 nm Ge quantum well on a $Si_{0.1}Ge_{0.9}$ virtual substrate with $Si_{0.15}Ge_{0.85}$ barriers as a function of electric field at 300 K. Curves at the bottom of the figure as calculated by 8-band **k**.**p** theory assuming a 0.2% tensile strained substrate and curves at the top of the figure are experimental data from Ref. 5. The theory and experimental curves are offset for clarity.

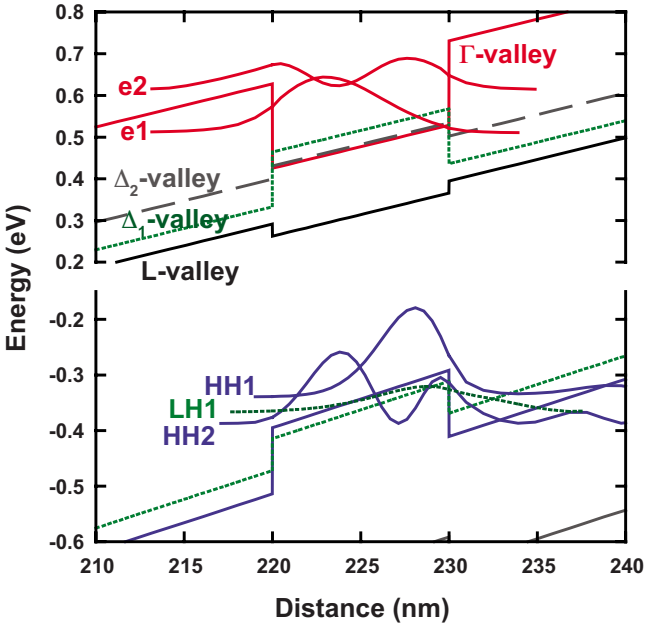

FIG. 7. (Color online) The band structure for 4 V applied (10.3 MV/m) to a 10 nm Ge quantum well with the Stark shift clearly evident for the squared wave functions of the lowest energy electron and hole states. The wave functions have been scaled to 2.5 times the height in Fig. 1 to aid clarity.

system. As the indirect transition is about 140 meV lower in energy than the direct transition, this will produce a tail below the direct HH1-e1 transition. To model this tail accurately will require another technique as the 8-band **k**.**p** technique is limited to direct transitions in the system.

The application of a Stark shift is expected to reduce the overlap of the electron and hole wave functions as the electric field is increased (see Fig. 7). To try to get a quantitative idea of the change in this overlap, the spatial overlap integral $\langle \psi^*_{HH1} | \psi_{e1} \rangle$ was calculated for the four experimental applied voltages from 0 to 4 V. To reduce boundary effects, the **k**.**p** solution to Schrödinger's equation was expanded to a distance of 50 nm each side of the quantum well. The results for the lowest subband states are plotted in Fig. 8 as a function of electric field. It is clear that the spatial overlap between the lowest electron and HH subbands reduces by a factor of 0.59 between 0 and 4 V applied across the *p*-*i*-*n* device. It should also be noted in Fig. 7 that the mixed LH/SO states are much more weakly confined than the HH states due to the lower heterostructure discontinuity. More detailed analysis of the modeled results suggests that by 4 V, only the lowest electron subband does not have any significant coupling to continuum states.

V. POLARIZATION DEPENDENCE OF ABSORPTION

All the experimental results published for Ge-quantum-well modulators have used the surface-normal *xy* polarization as this is the easiest to measure. There are many systems where waveguide geometry devices with *z* polarization (transverse magnetic) are useful. Figure 9 shows the absorption spectra for both *xy* and *z* polarizations for five different levels of tensile strained substrates calculated with the present 8-band **k**.**p** tool. The selection rules are, of course, different for the *z* polarization with the lowest dominant transition peak at flat bands being the LH/SO1-e1 transition with the HH1-e1 transition forbidden in the parabolic approximation.[11] The difference in selection rules results in the *z*-polarized absorption being at higher energy, although as the tensile strain in the substrate is increased, the difference between the *xy* and *z* polarizations is reduced as the LH/SO1 state becomes closer in energy to the HH1 state. If sufficient tensile strain could be applied (above approximately 0.6%), then for the present device, the *z* polarization

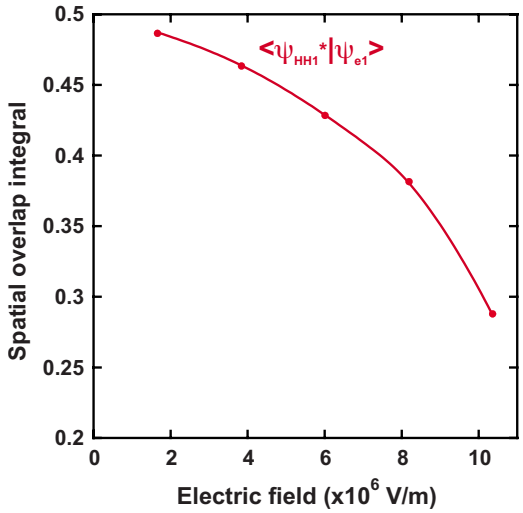

FIG. 8. (Color online) The spatial overlap integral between the lowest electron and lowest HH states as a function of electric field for a 10 nm Ge quantum well at 300 K. The values quoted are the mean for both spin states for each spin degenerate subband.

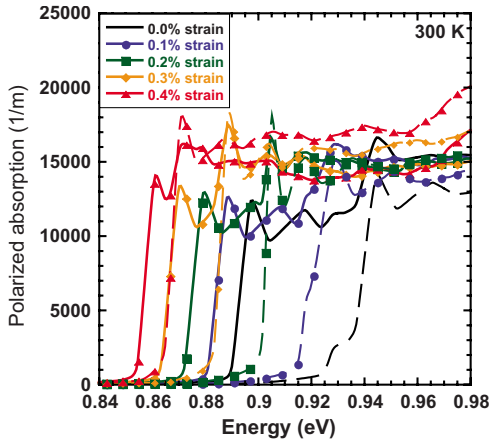

FIG. 9. (Color online) The calculated absorption spectrum at 300 K for a 10 nm Ge quantum well on a $Si_{0.1}Ge_{0.9}$ virtual substrate with $Si_{0.15}Ge_{0.85}$ barriers, an electric field of 1.63 MV/m at 300 K, and different levels of tensile strained substrate. Solid lines are *xy* polarization and dashed lines are *z* polarization.

would end up with a lower energy absorption edge when the LH/SO1 state is higher in electron energy (lower in hole energy) than the HH1 state. It is, however, not clear at present how such high levels of tensile strain could be achieved in a practical experimental device in the SiGe system.

Figure 10 shows the calculated *z*-polarized absorption spectrum for the 10 nm Ge-quantum-well device as a function of applied electric field in Ref. 6. The operation of the device is at higher energy (lower wavelength) than the *xy*-polarization device, but the shift in the excitonic absorption peak is much larger at lower electric fields. It is clear that for longer wavelength (lower energy) operation of a modulator different levels of Ge content, strain, and/or quantum well width are required if 1.55 μm operation is to be achieved.

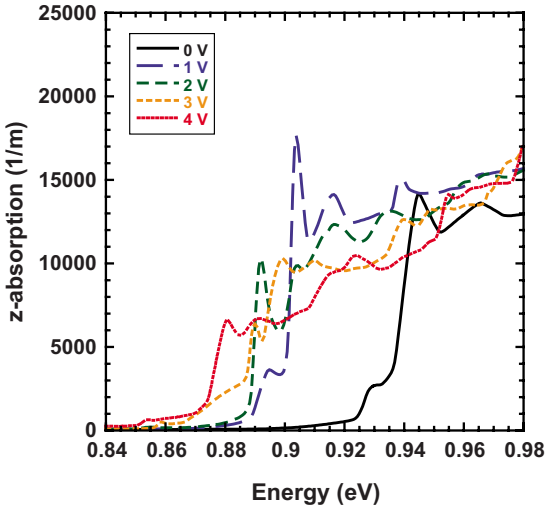

FIG. 10. (Color online) The *z*-polarized absorption spectrum at 300 K for a 10 nm Ge quantum well on a $Si_{0.1}Ge_{0.9}$ virtual substrate with $Si_{0.15}Ge_{0.85}$ barriers with voltage applied across a 460 nm *p-i-n* device region at 300 K. A 0.2% tensile strained substrate was assumed.

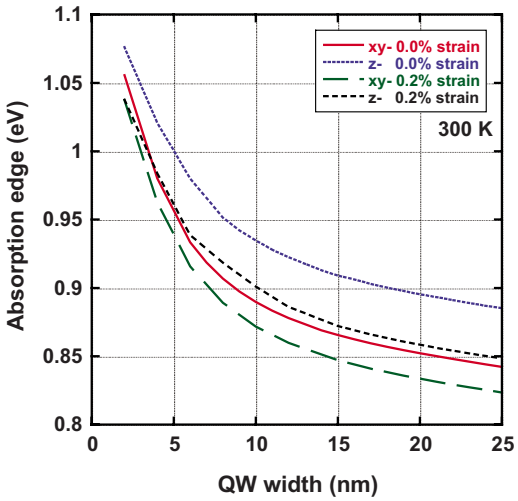

FIG. 11. (Color online) The absorption edge as a function of Ge-quantum-well width on $Si_{0.1}Ge_{0.9}$ virtual substrates with $Si_{0.15}Ge_{0.85}$ barriers with an electric field of 1.63 MV/m at 300 K.

VI. PREDICTIONS FOR GERMANIUM CONTENT AND QUANTUM WELL THICKNESS

In the final section of this paper, the 8-band $\mathbf{k}\cdot\mathbf{p}$ tool will be used to map out parts of the appropriate parameter space for making Ge-quantum-well QCSE modulators. The most important wavelength for photonics is 1.55 μm, which corresponds to 0.807 eV in energy. An ideal modulator would have the main absorption peak slightly higher in energy than 0.807 eV and be swept through this value to a lower energy with the application of a small applied bias. It is clear from the above results and as shown in Refs. 6 and 7 that a lower Ge content virtual substrate and wider quantum well are required for longer wavelength operation. Therefore, the absorption was calculated for different quantum well thicknesses for tensile strained and relaxed substrates of both $Si_{0.1}Ge_{0.9}$ and $Si_{0.05}Ge_{0.95}$ compositions. The results are plotted in Figs. 11 and 12.

To be consistent for both *xy*- and *z*-polarized calculations especially when strain in the substrate can result in anticross-

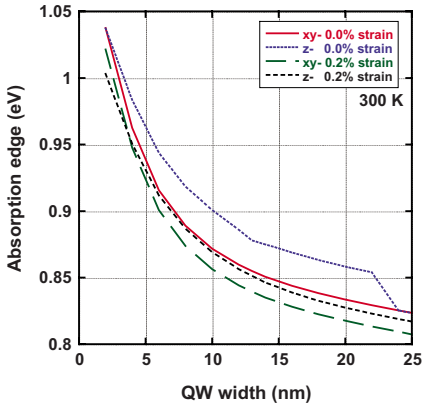

FIG. 12. (Color online) The absorption edge as a function of Ge-quantum-well width on $Si_{0.05}Ge_{0.95}$ virtual substrates with an electric field of 1.63 MV/m at 300 K.

ing of subband states, nonparabolicity, and mixing leading to multiple peaks near the absorption edge, the absorption edge has been defined as where the linear extrapolation of the lowest, distinct, direct-transition energy absorption peak edge crosses the energy axis. This may not be the best definition but does provide consistency to plot values on a single graph when band mixing of both HH and LH/SO states can relax the selection rules resulting in small absorption compared to the main exciton peak as can be observed in Fig. 10 for 1 V applied bias. The modeling results suggest that using a 0.2% tensile strained substrate of $Si_{0.05}Ge_{0.95}$ composition combined with a Ge quantum well of 15 nm or greater should allow modulation at 1.55 μm at 300 K in a low voltage device. Of course, operation of a device at higher temperatures will also result in longer wavelength operation due to the thermal shrinking of the band gap.[6,15] The wider quantum wells will also result in less spatial overlap of the wave functions and therefore there will be some maximum value of quantum well width above which the modulation with electric field will be too small to be useful due to the reduced absorption. Further modeling is required to determine this value and it is beyond the scope of the present paper.

VII. CONCLUSIONS

To conclude, an 8-band **k**.**p** tool has been used to model and simulate the absorption spectra of a number of Ge-quantum-well structures. To accurately agree with the experimental devices grown on thin virtual substrates, the substrates had to have tensile strain applied, while for thick graded buffers, the experimental results agree with theory without any strain in the virtual substrate. The excellent agreement between theory and experiment demonstrates that the direct band gap absorption dominates the device characteristics especially at low electric fields and low temperatures. The tool was also used to predict the performance of z-polarized waveguide geometry devices along with mapping out the useful energy space over which such modulators could be applied.

ACKNOWLEDGMENTS

The author would like to acknowledge the support of Stefan Birner with the NEXTNANO software along with useful discussions with Paul Stavrinou and Jing Zhang.

*d.paul@elec.gla.ac.uk

[1] R. A. Soref and B. R. Bennett, IEEE J. Quantum Electron. **QE23**, 123 (1987).
[2] R. A. Soref, Proc. IEEE **81**, 1687 (1993).
[3] A. Liu, R. Jones, L. Liao, D. Samara-Rubio, D. Rubin, O. Cohen, R. Nicolaescu, and M. Paniccia, Nature (London) **427**, 615 (2004).
[4] Q. Xu, B. Schmidt, S. Pradhan, and M. Lipson, Nature (London) **435**, 325 (2005).
[5] Y. H. Kuo, Y. K. Lee, Y. Ge, S. Ren, T. Kamins, D. A. B. Miller, and J. S. Harris, Nature (London) **437**, 1334 (2005).
[6] Y. H. Kuo, Y. K. Lee, Y. Ge, S. Ren, J. E. Roth, T. I. Kamins, D. A. B. Miller, and J. S. Harris, IEEE J. Sel. Top. Quantum Electron. **12**, 1503 (2006).
[7] D. A. B. Miller, D. S. Chemla, T. C. Damen, A. C. Gossard, W. Wiegmann, T. H. Wood, and C. A. Burrus, Phys. Rev. Lett. **53**, 2173 (1984).
[8] D. A. B. Miller, D. S. Chemla, T. C. Damen, A. C. Gossard, W. Wiegmann, T. H. Wood, and C. A. Burrus, Phys. Rev. B **32**, 1043 (1985).
[9] S. Tsujino, H. Sigg, G. Mussler, D. Chrastina, and H. von Känel, Appl. Phys. Lett. **89**, 262119 (2006).
[10] URL: http://www.wsi.tu-muenchen.de/nextnano3/
[11] G. Bastard, *Wave Mechanics Applied to Semiconductor Heterostructures* (Monograph de Physique, Paris, 1988).
[12] D. J. Paul, Semicond. Sci. Technol. **19**, R75 (2004).
[13] I. Vurgaftman, J. R. Meyer, and L. R. Ram-Mohan, J. Appl. Phys. **89**, 5815 (2001).
[14] *Semiconductor Physics: Group IV Elements and III-V Compounds*, edited by O. Madelung, M. Schultz, and H. Weiss, Landolt-Börnstein New Series, Group III, Vol. 17, Pt. A (Springer-Verlag, New York, 1982).
[15] Y. P. Varshni, Physica (Amsterdam) **34**, 149 (1968).
[16] C. G. van de Walle, Phys. Rev. B **39**, 1871 (1989).
[17] L. D. Laude, F. H. Pollak, and M. Cardona, Phys. Rev. B **3**, 2623 (1971).
[18] M. Chandrasekhar and F. H. Pollak, Phys. Rev. B **15**, 2127 (1977).
[19] S.-H. Wei and A. Zunger, Phys. Rev. B **60**, 5404 (1999).
[20] C. G. Van de Walle and R. M. Martin, Phys. Rev. B **34**, 5621 (1986).
[21] G. S. Cargill, J. Angilello, and K. L. Kavanagh, Phys. Rev. Lett. **61**, 1748 (1988).
[22] I. Balslev, Phys. Rev. **143**, 636 (1966).
[23] M. M. Rieger and P. Vogl, Phys. Rev. B **48**, 14276 (1993).
[24] R. W. Kelsall, Z. Ikonic, C. R. Pidgeon, P. J. Philips, P. Harrison, S. A. Lynch, P. Townsend, D. J. Paul, S. L. Liew, D. J. Norris. and A. G. Cullin, Phys. Rev. B **71**, 115326 (2005).
[25] S. A. Lynch, D. J. Paul, P. Townsend, G. Matmon, Z. Suet, R. Kelsall, Z. Ikonic, P. Harrison, J. Zhang, D. Norris, *et al.*, IEEE J. Sel. Top. Quantum Electron. **12**, 1570 (2006).
[26] M. Califano, N. Q. Vinh, P. J. Phillips, Z. Ikonic, R. W. Kelsall, P. Harrison, C. R. Pidgeon, B. N. Murdin, D. J. Paul, P. Townsend *et al.*, Phys. Rev. B **75**, 045338 (2007).
[27] T. Fromherz, M. Meduna, G. Bauer, A. Borak, C. V. Falub, S. Tsujino, H. Sigg, and D. Grützmacher, J. Appl. Phys. **98**, 044501 (2005).
[28] J. Liu, D. D. Cannon, K. Wada, Y. Ishikawa, D. T. Danielson, S. Jongthammanurak, J. Michel, and L. C. Kimerling, Phys. Rev. B **70**, 155309 (2004).
[29] J. Liu, D. Cannon, K. Wada, Y. Ishikawa, S. Jongthammanurak, D. T. Danielson, J. Michel, and L. C. Kimerling, Appl. Phys. Lett. **87**, 011110 (2005).